# Paper I

How to detect desert trees using CORONA images: Discovering historical ecological data

Journal of Arid Environments 65 (2006) 491–511

Journal of Arid Environments

www.elsevier.com/locate/jnlabr/yjare

# How to detect desert trees using CORONA images: Discovering historical ecological data

G.L. Andersen*

*Department of Biology, University of Bergen, Postboks 7800, N-5020 Bergen, Norway*

Received 31 March 2005; received in revised form 24 June 2005; accepted 15 July 2005
Available online 6 September 2005

**Abstract**

Lack of appropriate historical data has seriously impeded research into the extent and effects of deforestation in arid lands, but the declassification of CORONA satellite images has now made it possible to study long-term changes in arboreal vegetation. The potential and limitations of such images for long-term vegetation studies are scrutinized in the light of this research. High-resolution images (ca. 2.7 m) from 1965 are compared to field data (2003) of individually mapped wadi trees (*Acacia tortilis* and *Balanites aegyptiaca*) from 20 different sites in the Eastern Desert of Egypt. Of trees mapped in 2003 (canopy area (CA) $>6\,m^2$) 70% was detected in the imagery. A spatial classification shows that between 9% and 55% of the population was concealed by landscape elements that reduce image contrast. The study indicates that 97% of the population mapped in 2003 was already present in 1965 and that trees grow slowly and are older than previously assumed. Pollarded trees were detected in the imagery, and the resultant reduction in CA may lead to misinterpretations in change analyses.

CORONA images offer a spatial and temporal dimension for ecological information which other data sources cannot furnish at a comparable cost, coverage, resolution or accessibility.


*Keywords:* CORONA KH-4a; High-resolution imagery; Tree detection; *Acacia tortilis*; Change analysis; Eastern Desert of Egypt

*Tel.: +47 55583343.
*E-mail address:* Gidske.andersen@bio.uib.no.

0140-1963/$ - see front matter 
doi:10.1016/j.jaridenv.2005.07.010

## 1. Introduction

In 1995, data from the first generation US photo-reconnaissance satellite, CORONA, were declassified (Clinton, 1995). CORONA provides high-resolution panchromatic panorama data between 1960 and 1972. Large parts of the globe were covered, but focus was on former communist controlled areas, mainly the USSR (McDonald, 1995). Several camera systems, referred to by their KEYHOLE (KH) designator, were used during the CORONA program. Of these the most advanced, KH-4b, had its best resolution of 1.8 m at nadir. Today these images represent an invaluable potential for detailed, long-term environmental change analyses (McDonald, 1995).

CORONA data had important civilian applications before their declassification (McDonald, 1995; Cloud, 2001), and since 1995 several studies have applied these data to a range of applications, including archaeology, geomorphology, geology, forest and vegetation changes, for the generation of digital elevation models and orthophotos, and for general landscape studies (Tappan et al., 2000; Altmaier and Kany, 2002; Kostka, 2002; Philip et al., 2002; Goslee et al., 2003; Rigina, 2003; Fowler, 2004a, b; Lorenz, 2004; Sohn et al., 2004). In the study reported here, CORONA images were acquired for a project focusing on population dynamics of arid arboreal vegetation.

In arid African environments, trees are among the most important natural resources for pastoralists and their animals. In general, they represent the sole stable source of animal fodder, provide energy, shelter and shade, and act as a soil stabilizer (Alstad and Vetaas, 1994; Springuel and Mekki, 1994; Krzywinski and Pierce, 2001). The density of perennial species in arid areas of North Africa and the Middle East is, however, decreasing (Hobbs, 1989; Springuel and Mekki, 1994; Ward and Rohner, 1997; Christensen, 1998; Krzywinski and Pierce, 2001) and in the Eastern Desert of Egypt (ED) considered here this is mainly due to commercial charcoal and fuel wood production caused by high demand for energy. Despite the significant global focus on arid land vegetation changes (Thomas and Middleton, 1994), the degree and, in particular, the long-term consequences of this decrease are not well known. Because reliable detailed historical data have so far been scarce, the understanding of the long-term dynamics of perennial vegetation, e.g. trees, in arid and semi-arid environments is poor (Noy-Meir, 1979/80, 1985; Kenneni and van der Maarel, 1990; Wiegand et al., 1995; Wiegand and Milton, 1996; BenDavid-Novak and Schick, 1997; Martin and Moss, 1997; Ward and Rohner, 1997; Eshete and Stahl, 1999; Kadmon and Harari Kremer, 1999; Wiegand et al., 1999, 2000a, b; Wiegand and Jeltsch, 2000; Lahav-Ginott et al., 2001), and there is a lack of population structure data for even one species over many spatial and temporal conditions (Chesson et al., 2004).

The potential of aerial photos alone or in combination with high-resolution satellite images for studies of long-term vegetation changes in arid and semi-arid areas is acknowledged by many authors (Cole, 1989; Kadmon and Harari Kremer, 1999; Tappan et al., 2000; Lahav-Ginott et al., 2001; Laliberte et al., 2004). Goslee et al. (2003) use CORONA images from the 60s in combination with other aerial and satellite photos, for studying shrub encroachment in New Mexico, USA, but discard

the CORONA data from the analysis because these have poorer contrast and initial resolution than the remaining images. However, Tappan et al. (2000) point out that CORONA is a 'remarkable tool…even to the point of enumerating individual shrubs and trees in open field conditions'.

Although image quality varies, CORONA data are able to offer a spatial and temporal dimension to ecological information that is not available by other means comparable in price, coverage, resolution or accessibility. Therefore, in combination with later images or other types of spatial data they have a great potential not only to shed light on the degree of change over a rather long time period, but also on the poorly understood long-term dynamics of arid arboreal vegetation. However, as Goslee et al. (2003) also point out, in order to exploit this potential effectively it is important to understand the limitations of the image material. Only if these limitations can be described or quantified, is it possible to make good population estimates directly from the imagery.

The objective of the current study is to scrutinize the potential and limitations of CORONA imagery for the study of arid arboreal vegetation ecology and dynamics. The potential of CORONA images is assessed through applications on different scales: both as survey data sets on a landscape scale and as a data set on individual trees on a population scale. The study considers how far it is possible to go in interpreting the vegetation content of images and, on the population scale, to what degree it is possible to identify individual trees as well as what part of the population is identifiable and how this identification is influenced by landscape and image properties. Field observations gathered in 2003 in the ED will be used as reference data in the study.

### *1.1. Study area*

The study area in the ED is located between approximately the 24th and 25th parallels of latitude (Fig. 1). This area ranks among the most extreme deserts in the world (Meigs, 1953), and the coefficient of variation of rainfall reaches 200% (Andersen, 1999). In addition to scattered showers and oreographic rain, dewfall, mist and fog are important water sources (Ball, 1912; Hassib, 1950; Täckholm, 1969; Kassas and Zahran, 1971). The ED is a mountainous desert landscape, being part of the mountain range running parallel to the coast of the Red Sea. In combination with high mountain peaks (nearly 2000 m a.s.l.), the general proximity to the sea results in wide variation in the topo-hydrology of the mountain–valley (*wadi*) systems. It is in this widespread landform system that arboreal vegetation, i.e. *Acacia tortilis* (Forssk.) Hayne and *Balanites aegyptiaca* (L.) Del., grows and predominates (Table 1). Its persistence in the face of aridity is high since its roots are deeply seated in permanent soil moisture (Kassas, 1952, 1953, 1954; Batanouny, 1973; Zahran and Willis, 1992).

## 2. Material and methods

The procedure followed in order to achieve the objectives of the study includes five steps: (1) gathering field data; (2) image acquisition and scanning; (3) tree detection

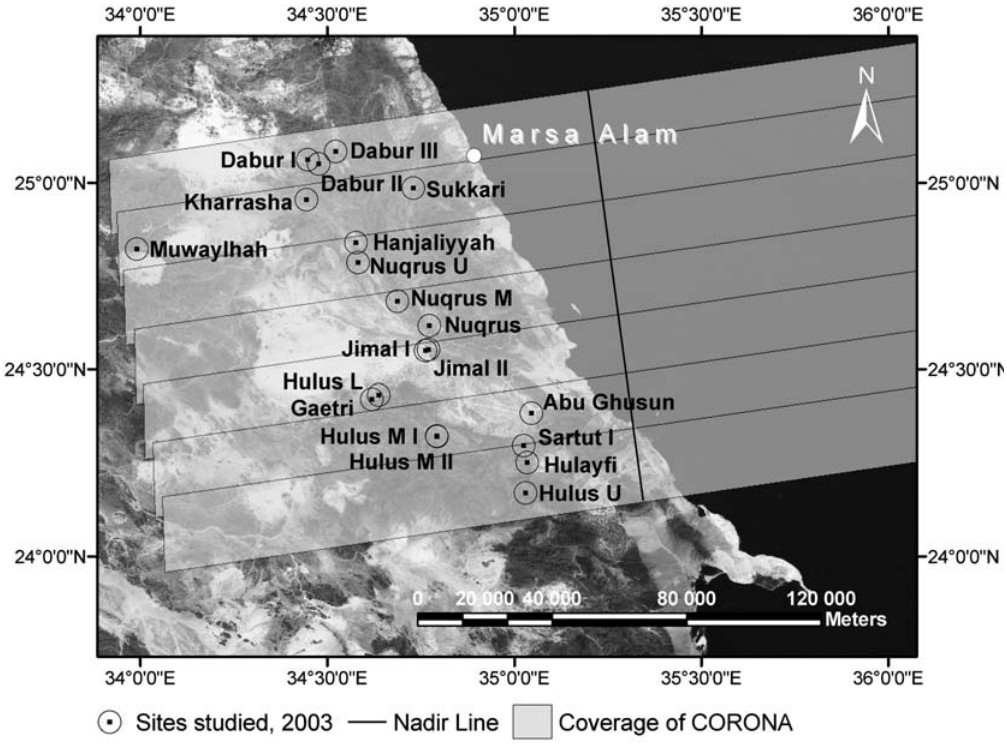


Fig. 1. Study area and distribution of sites studied in relation to coverage of CORONA images, overlaid on a Landsat TM image.

in CORONA imagery; (4) image rectification and (5) assessment of the accuracy of the tree detection in a spatial overlay with field data.

### 2.1. Field data

During fieldwork in February and March 2003 the arboreal vegetation on 20 sites (Table 1) located within the coverage of the imagery (Fig. 1) was mapped in detail. On each site individual trees (all sizes) were mapped using global positioning system (GPS) measurements. An external antenna, connected to the handheld GPS (Garmin 12XL), was mounted on an extendable pole to overcome poor reception under the canopies of trees. Several parameters describing the population structure were measured, and each tree was photographically documented. Canopy area (CA) was estimated by pacing (converted into metres) the greatest length of each canopy and the length orthogonal to it, and by assuming a mean circular shape. Traces of browsing and pollarding (Fig. 2) were also registered for each tree. Pollarding is a widespread and traditional management technique in the ED in which branches are harvested for fodder and firewood and to increase biomass production (Krzywinski and Pierce, 2001).

### 2.2. CORONA imagery and scanning

The images used in this project were acquired on 10 December 1965, at 10:53 Universal Time (KH-4a system, mission 1027-1, frames 142–148) by the forward

Table 1
Some characteristics of sites studied

| Sites | *Acacia tortilis* (*n*) | *Balanites aegyptiaca* (*n*) | Other species (*n*) | Individuals CA $>6\,m^2$ (*n*) | Mean CA $>6\,m^2$ | Density (tree/ha) | NNdist (mean) | NNdist (median) | Wadi orientation |
|---|---|---|---|---|---|---|---|---|---|
| Dabur I | 63 | 1 | 0 | 41 | 34 | 2.5 | 38 | 30 | 224 |
| Dabur II | 55 | 0 | 0 | 33 | 41 | 3.5 | 33 | 31 | 97 |
| Dabur III | 38 | 0 | 0 | 27 | 62 | 2.6 | 47 | 38 | 359 |
| Sukkari | 36 | 0 | 0 | 31 | 59 | 1.2 | 53 | 52 | 61 |
| Hanjaliyya | 37 | 0 | 0 | 30 | 50 | 0.9 | 54 | 30 | 256 |
| Kharrasha | 41 | 3 | 0 | 22 | 55 | 1.6 | 46 | 49 | 313 |
| Muwaylhah | 38 | 0 | 2 | 15 | 79 | 3.7 | 15 | 13 | 207 |
| Nuqrus U | 41 | 0 | 0 | 27 | 60 | 7.7 | 20 | 21 | 133 |
| Nuqrus M | 33 | 1 | 0 | 26 | 41 | 0.2 | 133 | 112 | 133 |
| Nuqrus | 35 | 7 | 1 | 38 | 128 | 1.5 | 48 | 43 | 126 |
| Hulus U | 68 | 0 | 1 | 23 | 49 | 26.5 | 15 | 13 | 197 |
| Hulus M | 34 | 0 | 0 | 26 | 47 | 8.0 | 26 | 22 | 358 |
| Hulus M II | 32 | 0 | 0 | 27 | 91 | 2.6 | 32 | 24 | 322 |
| Gaetri | 42 | 0 | 0 | 37 | 83 | 0.8 | 55 | 38 | 74 |
| Hulus L | 32 | 0 | 0 | 22 | 100 | 2.9 | 39 | 39 | 37 |
| Jimal I | 8 | 66 | 1 | 35 | 38 | 3.5 | 40 | 23 | 68 |
| Jimal II | 5 | 47 | 2 | 31 | 51 | 6.0 | 19 | 11 | 54 |
| Sartut I | 38 | 0 | 0 | 34 | 56 | 8.8 | 21 | 18 | 328 |
| Abu Ghusun | 44 | 0 | 0 | 37 | 74 | 3.0 | 36 | 32 | 38 |
| Hulayfi | 32 | 0 | 0 | 29 | 48 | 10.1 | 14 | 12 | 107 |
| Total | 752 | 125 | 7 | 591 | | | | | |

*Note*: L, M and U refer to lower, middle and upper, respectively. CA refers to canopy area. *Other species* include *Leptadenia pyrotechnica*, *Ochradenus baccatus*, *Acacia ehrenbergiana* and *Acacia etbaica*. *NNdist* refers to the nearest neighbour tree distance in metres. *Wadi orientation* is the dominant orientation in degrees from North of sites studied, measured along the flow direction of water.

Fig. 2. Pollarded tree: Branches are harvested for fodder and firewood and to increase biomass production (Krzywinski and Pierce, 2001). Pollarding is a widespread and traditional management technique and causes a substantial reduction in the canopy area of trees. Different degrees and stages of the practice can be seen in the Eastern Desert.

looking camera (cf. below) and were purchased as negative film. KH-4a was a constantly rotating stereo panoramic camera system, in which the two cameras had a separation angle of 30°. The film width used was 70 mm and the focal length 24 in. Each image covers an area of approximately $19.5 \times 266.5\,km^2$. Best resolution at nadir is 9 ft, but due to the nature of panoramic cameras this resolution significantly decreases towards the edges of the image (Lillesand and Kiefer, 2000; Sohn et al., 2004). As seen in Fig. 1, all sites are west of the nadir line, which means that the sun-camera geometry/constellation is comparable for all sites.

The CORONA negative film copies were scanned on a Nikon Coolscan 8000 AD scanner, at a spatial resolution of 4000 dpi (6.35 μm) and a radiometric of 14 bits (later transformed to 16 bits). This high spatial resolution is required in order to obtain digital images with a resolution at nadir close to the film resolution of 9 ft (2.7 m). Because the negatives are long strips (about $75 \times 5\,cm^2$) they were cut into several sub-images that were scanned separately.

### 2.3. *Tree detection in CORONA imagery*

In the CORONA images used for this study trees appear as dark rounded to oval dots. The shadows of their canopies contribute to this appearance (Campbell, 2002). The size of the shadow on the image is given not only by the size of the canopy and

its height above the ground but also by the sun-camera geometry (Strahler and Jupp, 1990). The brightness of the image structure is related to the density of the canopy (number of branches and leaves). The brightness of the background is influenced by the type of soil material and its texture. A successful recognition of trees requires good contrast between canopy (+shadow) and background. Obviously, the film resolution (120 l/mm) is a main factor influencing the ability to recognize trees, and this resolution is strongly affected by contrast. The spatial resolution of the total photographic system is influenced by several factors external to the system itself (e.g. camera vibrations) that cause the spatial resolution of the images to vary, i.e. that the spatial resolution becomes dynamic (Lillesand and Kiefer, 2000).

The properties of CORONA images have not previously been explored for tree detection, and consequently a verified automatic procedure is not available. In a first approach to tree detection, the most accurate method for identification should be applied. Since human vision is well prepared for pattern recognition and therefore for image interpretation, a visual image interpretation was adopted.

In the interpretation process, each tree-like structure was digitized manually and represented by a point since no attempts to estimate CA, i.e. delineate it, are made. These points are referred to as 'interpreted' trees. The visual interpretation of the images was done independently of the field data, i.e. before the rectification of the images, in order to obtain results comparable to a situation where reference data are absent. Each site's distance from the nadir line of the image is calculated as one indicator of actual spatial resolution.

### 2.4. *Rectification of CORONA imagery*

The images were rectified in ArcGIS™ using all mapped trees (2003) as potential reference data. Each tree mapped in the field is displayed with a symbol proportional in size to its CA because this makes it easier to recognize individual trees on the imagery. For each ground control point (GCP) added in the rectification process ArcMap automatically updates the transformation on the screen, thus making it possible visually to judge the result as the set of GCPs is changed. Since the true error of each individual position is unknown, the sampling to obtain an optimal set of GCPs was done iteratively by 'trial and error' until the root mean square (RMS) error was minimized at the same time as the fit between the image and the full reference data set was maximized. The fit was assessed visually. A linear transformation was used for the rectification since each site image covers a relatively small area. The resampling applied was nearest neighbour. Digitized points (i.e. interpreted trees) for each site were geometrically corrected using the same GCPs as for the image rectification.

### 2.5. *Accuracy assessment of the tree detection*

The ability to detect trees from CORONA data was evaluated using a spatial overlay of interpreted CORONA maps (1965) and mapped field data (2003). Ground truth data from 1965 would be needed to assess fully the accuracy of the interpretation made,

but contemporaneous data are normally not available for historical images, as is the case here. To use 2003 data as reference data one assumption has to be made; namely, that at least the larger trees recorded in 2003 must have been present in 1965, and at a detectable size. This assumption was confirmed during fieldwork; several individual trees at sites studied were recognized in imagery (cf. below and Fig. 3). It is therefore possible to make accuracy estimates based on the population present in 2003. It is also possible to estimate the omission error. The part of the interpreted 1965 population that does not correspond to any present individual is either a tree which has disappeared or a misinterpretation, i.e. an error of commission, and cannot be further assessed by the approach adopted here.

Individuals in the reference data (2003) are labelled either as a 'recognized tree' or as an 'unrecognized tree' with reference to the 'interpreted' trees (1965). This labelling depends on the following assumptions:

1. Due to GPS errors and errors resulting from the rectification process there is a spatial discrepancy between trees mapped from CORONA images and trees mapped in the field. Hence, for any tree-point in one data set to be considered as referring to the same tree in the other data set, the two have to be closer to each other in the spatial overlay than any other two points and be separated by no more than 20 m. The threshold of 20 m is chosen in order to absorb the accumulated spatial error.
2. Trees present in 1965 that are below a threshold size will not generate a distinguishable signature in the imagery. An absolute threshold is the area of the pixel itself; but because the shadow of a canopy contributes to a trees' signature, a tree slightly smaller than one pixel might still be recognized. Adding to this is also the fact that objects smaller than ground resolution can be detected in digital images under optimal contrast conditions (e.g. roads, bridges, etc.). At most sites a portion of the tree population is below this minimum detectable size (Table 1). It is assumed that trees that were smaller than this size in 2003 cannot be detected in 1965 imagery. The threshold used was a CA of 6 $m^2$.

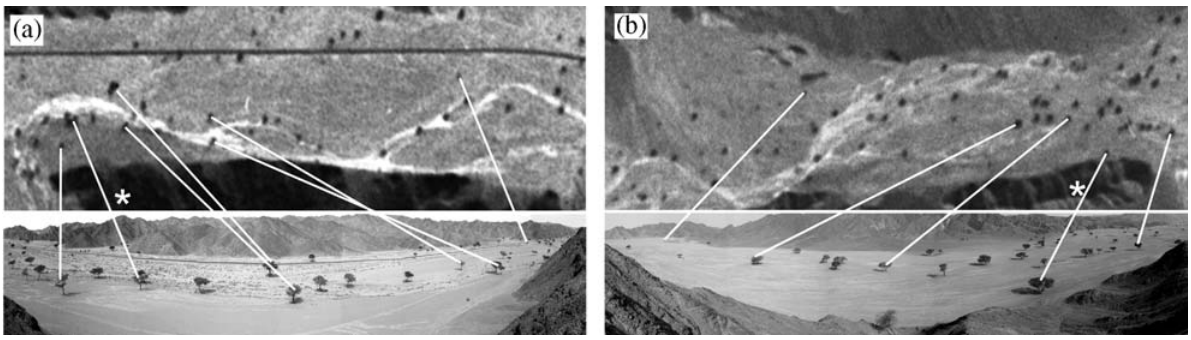


Fig. 3. Upper part of each illustration shows CORONA data from Wadi Dabur II (a) and Wadi Gaetri (b). Asterisks indicate locations from which panoramic images (lower part) were photographed. On CORONA images trees appear as dark rounded to oval dots. White lines show the spatial relation between the two images and the ability to recognize trees present in the historic images. It is easily seen that several trees are gone from the western (left) part of Wadi Gaetri.

A 'recognized tree' is then, by definition, a tree mapped in 2003 with a $CA > 6\,m^2$ and at a distance from interpreted trees (1965) $\leqslant 20\,m$ and an 'unrecognized tree' is a tree mapped in 2003 with $CA > 6\,m^2$ and at a distance from interpreted trees (1965) $> 20\,m$.

The latter group, whose members were in fact present in 2003 but were not recognized in the 1965 imagery, pose a problem. Two possibilities are envisioned; either they were present in 1965 but were unrecognizable in the imagery or they were not yet present but were recruited subsequently. In order to explain why signatures of members of this group that were present could not be detected, all its members were further classified according to a set of spatial criteria which are known to reduce image contrast and consequently interpretability of imagery (cf. 2.3). The threshold of 20 m is used for the reasons mentioned above. The spatial classification for unrecognized trees is as follows:

- $N_1$: The distance from present, larger ($CA > 6\,m^2$) trees are less than 20 m.
- $N_2$: At most sites in this mountainous environment there is a distinct difference in brightness between the sandy to stony bed of a wadi, where trees are growing, and the adjacent mountains. Normally, a wadi bed is much brighter than its surroundings. In this class, the distance from a dark–bright transition is less than 20 m.
- $N_3$: The distance from other recognized dark structures within a site is less than 20 m. Dark structures within a site can be, e.g. larger rocks, inselbergs or a tree that is not recognized during visual interpretation.
- $N_0$: Distance from any of the above-mentioned objects is more than 20 m; i.e. individuals remain unrecognized.

Objects in classes $N_2$ and $N_3$ are recognized by dividing image digital numbers (DNs) into two intervals separated by a threshold value, i.e. level slicing (Lillesand and Kiefer, 2000). The threshold value used is estimated from spectral profiles across each site, including both the wadi bed and the mountainsides. Different thresholds, given in Table 2, are applied, mainly because the geology and type of soil material and size of its constituents vary among sites. However, photographic conditions during image acquisition, e.g. film exposure, and/or contrast stretching during scanning can also influence the differences among sites.

## 3. Results

### 3.1. CORONA as a data set for surveys

In the study area, as in many arid areas, infrastructure is poorly developed and fieldwork, survey or even travel can therefore be difficult and time consuming. It is extremely useful to have the opportunity to get a view of the conditions at a pre-selected site and in this sense CORONA can help in planning an optimal selection of sites for fieldwork. In this study, simple measures (i.a. presence versus absence of

Table 2
Some image characteristics for the sites studied

| Sites | Pixel size (m) | RMS error (m) | Threshold value for level slicing (DN) | Distance from nadir line (%) |
|---|---|---|---|---|
| Dabur I | 2.8 | 8.0 | 20,000 | 60 |
| Dabur II | 2.6 | 8.7 | 20,000 | 57 |
| Dabur III | 2.6 | 2.3 | 20,000 | 54 |
| Sukkari | 2.5 | 1.2 | 25,000 | 39 |
| Hanjaliyya | 2.7 | 5.2 | 25,000 | 52 |
| Kharrasha | 2.6 | 5.5 | 30,000 | 62 |
| Muwaylhah | — | — | — | 95 |
| Nuqrus U | 2.5 | 4.3 | 25,000 | 52 |
| Nuqrus M | 2.6 | 3.6 | 25,000 | 46 |
| Nuqrus | 2.5 | 8.8 | 20,000 | 39 |
| Hulus U | 2.6 | 10.2 | 30,000 | 25 |
| Hulus M I | 2.9 | 5.9 | 20,000 | 42 |
| Hulus M II | 3.1 | 8.4 | 30,000 | 42 |
| Gaetri | 2.7 | 3.4 | 20,000 | 54 |
| Hulus L | 2.7 | 3.4 | 20,000 | 52 |
| Jimal I | 2.5 | 6.8 | 40,000 | 42 |
| Jimal II | 2.4 | 7.9 | 40,000 | 42 |
| Sartut I | 2.5 | 2.7 | 40,000 | 26 |
| Abu Ghusun | 2.5 | 4.8 | 40,000 | 22 |
| Hulayfi | 2.5 | 6.7 | 35,000 | 25 |

*Note*: *Distance from nadir line* is the distance between nadir and site studied in per cent of the total distance from nadir to the edge of the image. *RMS error* is the root mean square error of the rectification. Threshold value is given in digital numbers (DN), ranging over the 16 bit radiometric resolution used in the image processing (0–65,535).

arboreal vegetation or, at a more informative level, the density of vegetation) furnished practical information extracted from the raw digital imagery. Such information also helps in the formulation of working hypotheses and can give rise to new ones.

In the field, images contribute important information on a larger scale, e.g. by making possible a firm estimate of the changes that have occurred at a particular site in the period since image acquisition. The simplest method is to compare the number of trees on the site with number of trees within the same boundaries on the imagery. Individual trees can also be identified as long as it is possible to get an overview of the landscape, e.g. from a low elevation (Fig. 3). This approach is difficult in large open areas where there are few landscape elements to use as reference points or when the vegetation density is too high.

### 3.2. CORONA as digital maps

Scanning at 4000 dpi gives a pixel size after geometric correction ranging between 2.4 and 3.1 m (Table 2), i.e. it retains the best spatial resolution of the imagery.

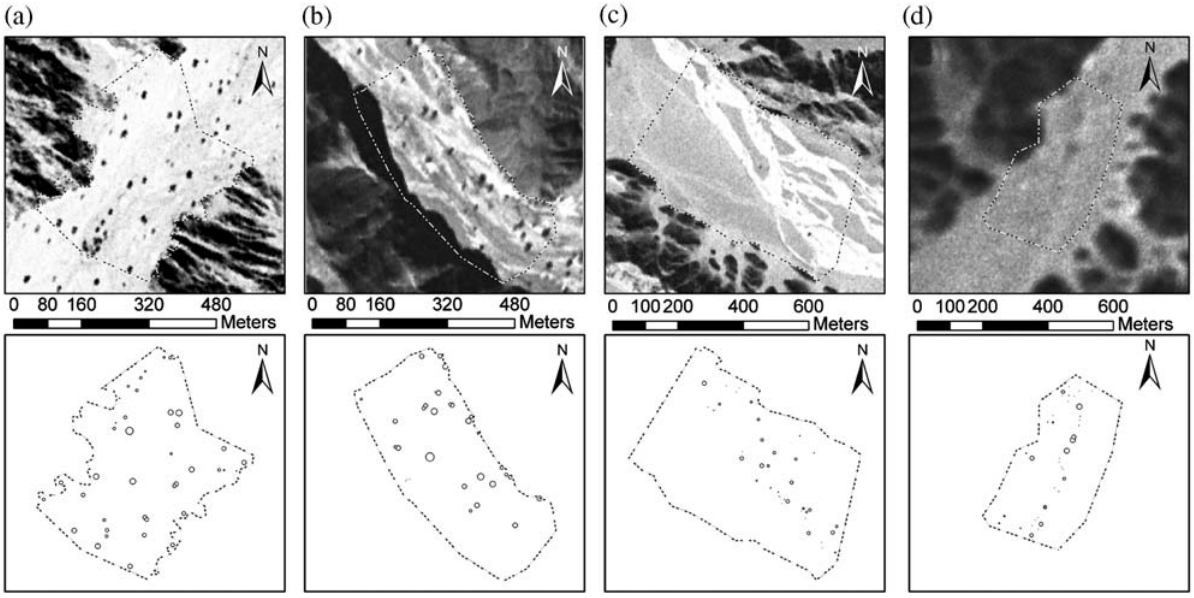


Fig. 4. Effect of distance from the nadir line on resolution (specified in brackets, cf. Table 2): (a) Wadi Abu Ghusun (22%), (b) Wadi Hulus MII (42%), (c) Wadi Kharrasha (62%) and (d) Wadi Muwaylhah (95%). The upper panel shows rectified CORONA imagery, where a dotted line indicates the extent of the area mapped in the field. The lower panel shows individual trees registered during fieldwork 2003. The size of the symbol is proportional to the canopy area of trees. While features in (c) are less clear than in (a) and (b), the resolution in (d) is so low that no trees can be detected, regardless of their size.

Distance from the nadir line (Table 2) gives an indication of the actual resolution of the site image. Sites further away from the nadir line have an increasingly poorer resolution than sites close to it (cf. above and Fig. 4). For one site, Wadi Muwaylhah, located furthest from the nadir line (Table 2: distance from nadir line), the resolution is too coarse to detect any trees at all (Fig. 4d), and the site image could therefore be neither interpreted nor rectified as described above. This site is therefore excluded from the results discussed below.

The RMS error for the rectification of site images ranges between 1.2 and 10.2 m (Table 2). Because the same GCPs are used for the spatial adjustment of the interpreted points as for the rectification, the same errors arise.

Only the image of the Wadi Hulayfi site was problematic to rectify. At this site several factors accumulated to decrease the ability to recognize individual trees. Vegetation density is high (Table 1), and coarse wadi substrate reduces the ability to recognize individual trees. In addition, it is situated in a narrow wadi close to the G. Hamata massif, increasing the risk of multi-pathing, i.e. the reflection of signals from other objects altering the signal received, and poor GPS readings. The latter is also the case for Wadi Hulus upper which has the highest RMS error. There, however, a few easily recognizable larger trees made the rectification possible.

### *3.3. Tree detection and accuracy assessment*

Working both with CORONA imagery in the field and in the rectification process shows that mature individual trees present in 2003 are recognizable on the images

from 1965. Indeed, the spatial overlay shows that 382 individuals (66%, Table 3) of the 576 individuals registered in field ($CA > 6\,m^2$, Table 1, excluding Wadi Muwaylhah) are recognizable on the imagery. In all, 766 individuals were interpreted visually on the imagery (cf. Section 2.3). Of recognized trees 84% are within 10 m and 97% within 15 m of the nearest interpreted tree, while the grand median and mean nearest neighbour distances between larger trees ($CA > 6\,m^2$) are 27 and 40 m, respectively (Table 1, Rowlingson and Diggle, 1993).

In addition to obtaining an overview of the historical presence of trees, it is also possible to gain an impression of their sizes. Although no attempt has been made to delineate the CAs of interpreted structures, a visual inspection of imagery shows that relative differences in size among neighbouring individuals today are similar to what they were in 1965, e.g. smaller trees today correspond to smaller or less distinct structures in the 1965 imagery, while trees large in 2003 were also relatively larger

Table 3
Results from the spatial overlay of field data (2003) and image interpretation (1965)

| Sites | Individuals (2003) | | Unrecognized (spatially classified) | | | |
|---|---|---|---|---|---|---|
| | Recognized | Unrecognized | $N_0$ | $N_1$ | $N_2$ | $N_3$ |
| Dabur I | 29 | 12 | 1 | | | 11 |
| Dabur II | 26 | 7 [1] | 3 | | 4 | |
| Dabur III | 19 | 8 [1] | 1 | | 5 | 2 |
| Sukkari | 16 | 15 [1] | 3 | | 9 | 3 |
| Hanjaliyya | 22 | 8 [1] | 1 | 1 | 6 | |
| Kharasha | 12 | 10 [4] | 9 | 1 | | |
| Nuqrus U | 16 | 11 [2] | 4 | | 2 | 5 |
| Nuqrus M | 16 | 10 [2] | 3 | | 5 | 2 |
| Nuqrus | 28 | 10 | 1 | 1 | 4 | 4 |
| Hulus U | 12 | 11 [4] | 2 | 2 | 4 | 3 |
| Hulus M | 18 | 8 [1] | | | 7 | 1 |
| Hulus M II | 16 | 11 | | | 5 | 6 |
| Gaetri | 29 | 8 | 1 | | 5 | 2 |
| Hulus L | 11 | 11 [1] | 1 | | 7 | 3 |
| Jimal I | 32 | 3 | | | 3 | |
| Jimal II | 14 | 17 | | 4 | 8 | 5 |
| Sartut I | 23 | 11 [3] | | 3 | 7 | 1 |
| Abu Ghusun | 26 | 11 [1] | | 2 | 6 | 3 |
| Hulayfi | 17 | 12 | | 4 | 1 | 7 |
| Total ($n$) | 382 (+22) | 194 (−22) | 30 (−11) | 18 (−4) | 88 (−6) | 58(−1) |
| Total (%) | 66.3 (70.1) | 33.7 (29.9) | 5.2 (3.3) | 3.1 (2.4) | 15.3 (14.2) | 10.1 (9.9) |

*Note*: *Recognized* refers to individuals present in 2003 and detected in 1965 imagery. *Unrecognized* refers to individuals present in 2003 but not detected in the imagery. Numbers in square brackets refer to the number of individuals that were relabelled to recognized after a visual reinspection of the imagery, when field data from 2003 were overlaid on imagery. In all, 22 individuals (number in parenthesis) were relabelled after this visual reinspection. Unrecognized is further divided into $N_0$–$N_3$ based on a spatial classification (see main text). Only 3% ($N_0$) remain inexplicable after this classification and relabelling.

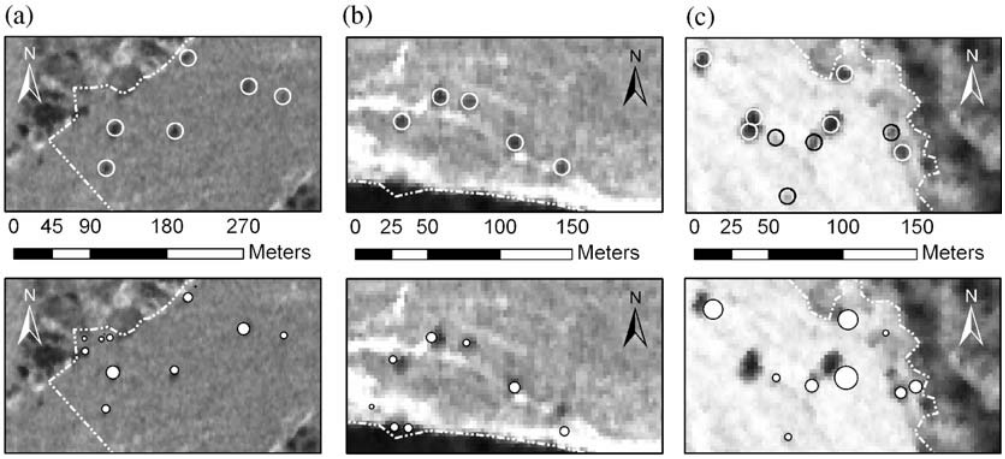


Fig. 5. Information on tree size in imagery: sections of (a) Wadi Sukkari, (b) Wadi Dabur II and (c) Wadi Sartut. Structures interpreted as trees (from 1965 imagery) are outlined (upper panel), overlaid on rectified imagery. Lower panel shows mapped trees (field data from 2003), with symbol size equal to canopy area (CA), overlaid on rectified imagery. The correlation between tree CA and size of interpreted image structure is seen. It is also worth noting the effect of substrate colour on the interpretability of imagery, e.g. the dark substrate in (a) reduces the contrast in the image and therefore the ability to recognize trees. In (a) and (b) there are also seen examples of omitted trees close to the mountain–wadi transition zone and of the increased interpretability when displaying field data on top of rectified imagery. This figure also gives an impression of the spatial accuracy of the rectification process.

then (Fig. 5). However, the effect of pollarding (Fig. 2) has also been detected using the spatial overlay. Some of the distinct and larger structures in the 1965 imagery coincide spatially with individuals that had a small CA in 2003. Five small individuals, located at sites Dabur I, Jimal I and II and Sartut, whose CA in 2003 was between 6 and 10 $m^2$ were recognized in imagery (1965). But this gives a false impression of minimum detectable size since a closer inspection of photos taken in 2003 shows that all of these individuals had been pollarded and probably had a larger CA in 1965.

There are 194 unrecognized trees (Table 3), excluding those individuals below the selected size limit (273). Of these 194 trees, 80% are within a 15 m distance and 85% are within a 20 m distance of landscape elements that reduce image contrast (cf. classes $N_1-N_3$). When it comes to CA only 5% of the recognized individuals were in the range 6–15 $m^2$, while 22% of the unrecognized $N_3$ individuals (close to other dark structures, cf. Section 2.3) is in this size class. Only 5% of the individuals remain unexplained ($N_0$) after this categorization.

All images were reinspected and compared with field data overlaid in order to check the explanatory power of the spatial classification scheme applied to unrecognized trees. In this exercise, 22 unrecognized trees could be relabelled as recognized, half of them having originally been in the $N_0$ category (Table 3). It is obvious that displaying field data on top of a rectified image makes it possible to detect image structures referring to trees that would otherwise be interpreted as background heterogeneity (Fig. 5). This is in particular the case at Wadi Hulus upper, where the interpretation has been too conservative. Also the selected threshold for level slicing was too conservative for this site. At other sites a few relatively distinct structures have simply

been overlooked (Wadi Dabur II and Dabur III). At the Kharrasha site (Fig. 4) several (large) individuals were in the $N_0$ category (Table 3). A gamma contrast stretch together with displaying field data on top of the image made it possible to reveal some of the unrecognized individuals, although they remained indistinct. It seems to be the case that this site has a poorer contrast and resolution than, e.g. Dabur I and II, which are approximately as far from nadir (Table 2). Whether the reason for this is technical features specific to filmstrip, properties specific to this site (bright background), or sun-camera geometry remains unclear.

Whatever the cause, 19 individuals (3%) of all larger trees ($CA > 6\,m^2$) mapped in 2003 remain inexplicable ($N_0$: Table 3). While it seems possible that the smaller of these were not there or were at least below the minimum detectable size in 1965, it is harder to explain why the larger individuals have not been recognized. A closer inspection of photos taken in field shows that thin foliage in combination with heterogeneous background can be an explanation for some missing individuals; but it still seems very likely that pollarding may be the main explanation for others. In these cases, pollarding before 1965 can have reduced canopy and therefore obscured the individuals' image signature. Since these individuals were already large in 1965, a significant canopy can have been re-established before mapping in 2003.

Looking in more detail at sites, the percentage of recognized trees, without any corrections, ranges from 45% at Jimal II to 91% at Jimal I (Fig. 6). As a matter of fact these sites are very similar when it comes to photographic properties. However, at Jimal II several trees are located close to the mountainside and a further complication for the detection of individuals is the shorter distance between them (Table 1), suggesting that one structure in the image might in reality refer to several trees.

The problem of trees concealed either by mountainsides or by other trees arises at all sites. The more severely negative influence of mountains on the detectability of trees is a function of the particular wadi's topography and orientation (Table 1) in relation to solar azimuth angle. As for the influence of background brightness, this is less when trees are larger, as, e.g. in Gaetri and Nuqrus, which are dominated by very large individuals (Table 1). There the percentage of recognized trees is close to 80% (Fig. 6). Small trees are more easily recognized on bright than on dark backgrounds. However, since factors that influence detectability are correlated, and since background brightness varies within sites, it is difficult to generalize at the site level.

## 4. Discussion and conclusion

CORONA is a useful tool for surveying a landscape, even without a geometric correction (Kostka, 2002) and is a useful substitute for detailed aerial photos. In order to gain an overview of an area comparable in size to that covered by a single CORONA image one would have to acquire a large number of aerial photos, if such were available at all, or would have to use satellite imagery with a much poorer resolution. Satellite imagery with comparable resolution (e.g. IKONOS) which would make it possible to detect individual trees is far from comparable in coverage, not to mention in price.

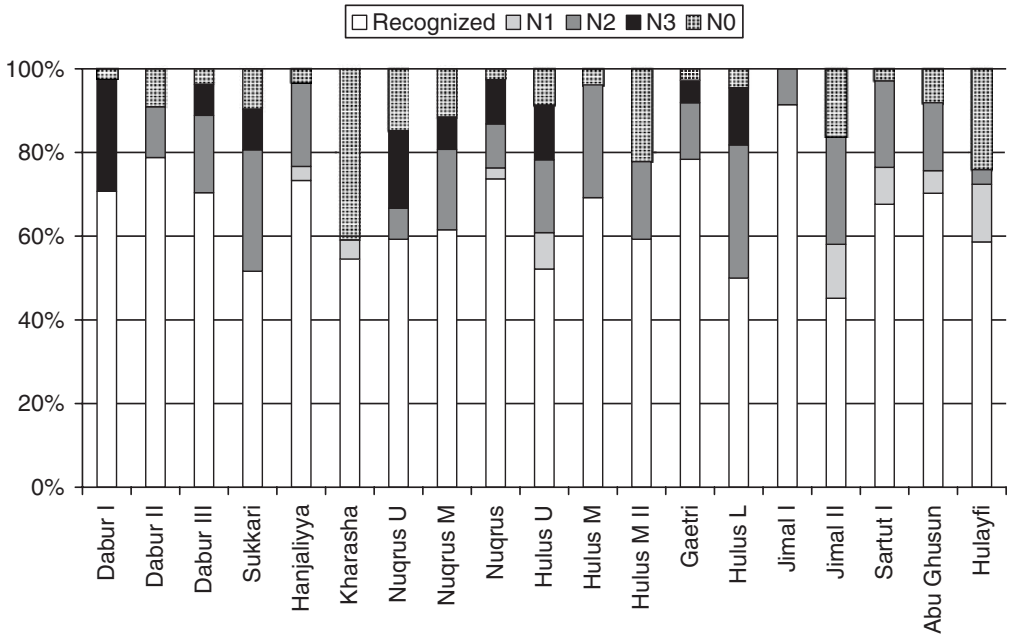


Fig. 6. Shows how recognized and unrecognized trees (2003) are distributed (%) at the different sites studied (before relabelling, cf. Table 3). A 'recognized tree' is a tree mapped in 2003 with a canopy area (CA) $>6\,m^2$ and distance from interpreted trees (1965) $\leqslant 20\,m$ and an 'unrecognized tree' is a tree mapped in 2003 with CA $>6\,m^2$ and distance from interpreted trees (1965) $>20\,m$. Unrecognized trees, i.e. $N_0-N_3$, are shown according to the results of the spatial classification.

Previously, CORONA images could be purchased as negative or positive film copies or as prints from the EROS Data Center, which one digitized according to one's own needs. Now the only option is a digital product, delivered as three files per scene (each 400 Mb) and with a resolution of 3600 dpi (7 μm, for both KH-4a and -4b). This resolution is higher than that used in other studies (Altmaier and Kany, 2002; Philip et al., 2002; Rigina, 2003; Fowler, 2004b; Lorenz, 2004), but for lossless digitalization of CORONA a resolution of 4 μm is recommended (Leachtenauer et al., 1998). Although scanning images oneself is time consuming (Leachtenauer et al., 1998), it permits optimal selection of spatial and radiometric resolution and greater flexibility when it comes to optimal stretching of the imagery. In cases where the methods used depend on pixel values, e.g. level slicing or unsupervised classification, and include comparison among several sub-images scanned separately, it would be necessary for a standardized stretching procedure during scanning process, e.g. using black and transparent reference areas. Further corrections are needed when large differences due to exposure occur (Kadmon and Harari Kremer, 1999; Rigina, 2003).

The geometric correction of CORONA images is difficult (Tappan et al., 2000; Rigina, 2003; Lorenz, 2004) due to several types of geometric distortion (Sohn et al., 2004). Altmaier and Kany (2002) and Sohn et al. (2004) have used traditional photogrammetric methods and mathematical modelling, respectively, for geometric correction and DEM generation. While this clearly offers exciting opportunities for correcting a complete scene (e.g. for detailed tree mapping over large areas), both

these studies mention the difficulties of collecting high quality and evenly distributed GCPs for such large areas.

The present study shows clearly that a simple geometric rectification, using GPS positions of trees as GCPs, gives acceptable results when smaller site images are rectified separately (Fig. 5). Improved accuracy can be achieved with Differential GPS (DGPS) measurements, but the equipment needed is more expensive and often less user friendly (Adrados et al., 2002). Operationalised DGPS services are offered in some areas (Butler and Ali, 2000) but are not easily available worldwide. After selective availability was terminated (Clinton, 2000), the (non-differential) GPS position accuracy of the standard positioning service has improved significantly (Adrados et al., 2002; IGEB, 2003). According to D'Eon et al. (2002) there is a 50% probability that GPS measurements will be within 5.9 m of the real position and a 95% probability that it will be within 30.6 m. Other authors (Hengl et al., 2001; Liu, 2002) have reported similar or even smaller errors. The results from the spatial overlay in the present study show that position accuracy lies within comparable ranges, including the possible effect of multi-pathing and bad geometry/satellite constellation. Such effects cannot, however, be corrected by DGPS measurements. Since the spatial error is less than the distance between trees, the spatial accuracy of rectified imagery and GPS measurements is sufficient for successful spatial overlay, and consequently also for change analysis.

The visual interpretation done in this study only attempted to detect trees, not to estimate their size; but because images clearly convey information about the size of trees (Fig. 5), methods that also delineate structures should be tested on CORONA imagery. Traditionally, the delineation of vegetation structures on aerial photographs has been performed manually. Kadmon and Harari Kremer (1999) recognize lack of consistency and lack of efficiency as disadvantages inherent in that approach. Several semi-automatic or automatic procedures for delineating individual canopies have been developed (Brandtberg and Walter, 1998; Larsen and Rudemo, 1998; Lahav-Ginott et al., 2001; Pouliot et al., 2002; Goslee et al., 2003; Laliberte et al., 2004; Wulder et al., 2004). Some are based upon a physical model of the geometric—optical properties of trees, and model inversion can give good estimates of different tree size parameters (Li and Strahler, 1985, 1986; Strahler and Jupp, 1990). Among the simpler approaches to tree detection and delineation is spectral classification or level slicing (Kadmon and Harari Kremer, 1999; Lillesand and Kiefer, 2000; Lahav-Ginott et al., 2001). Goslee et al. (2003) developed a semi-manual approach, where shrubs were first manually digitized as points and thereafter automatically delineated by an iterative algorithm which started from the digitized point and increased the estimated size until an edge difference value was reached. Laliberte et al. (2004) use an automatic segmentation algorithm. Because algorithms that are not physically based do not attempt to correct canopy size for the shadow effect (Campbell, 2002), canopy might be overestimated in panchromatic imagery. This effect depends not only on the shape and size of the tree itself but also on the zenith and azimuth angle of the camera and the sun (Strahler and Jupp, 1990). Collateral material (orbit and ephemeris data) for CORONA can be purchased from the National Archives.[1]

[1]8601 Adelphi Rd., College Park, MD 20740, USA.

A few small trees were recognized in the visual interpretation. A larger proportion of small individuals was categorized as $N_3$ (close to other dark structures), and this indicates that trees present in 1965 remained undetected by the visual interpretation, i.e. that the image interpretation was too conservative for small trees. The advantage of simple level slicing or other automatic procedures compared to a visual approach is that all interpretations are done in a consistent manner. However, results based on simple level slicing are highly dependent on the threshold selected, and easily include a high error of omission and/or commission as exemplified in the current detection and delineation of dark objects, e.g. Hulus upper site where the threshold selected was too conservative owing to low image contrast. Because a background can be highly heterogeneous, a dynamic threshold value for the delineation of objects could prove more appropriate.

Concealed individuals cannot, regardless of methodology, be detected since landscape properties or other trees obscure their presence in imagery. The results from a study like this can be used to estimate the probability of omitting trees in areas dominated by landscape elements that reduce image contrast. Hence, it is possible to make good estimates of actual population size even in areas where reference data are lacking, as long as landscape characteristics are similar. Even if it is not possible to estimate a probability of omitting trees, the result from a study like this will still be useful since it permits an optimal delineation of study sites by excluding areas where no or only poor estimates of actual population size are likely.

Since reference data from 1965 are lacking, it is impossible to estimate the number of misinterpreted trees, i.e. the commission error arising from the manual interpretation. This is important to consider since it will influence the results and reliability of a change analysis. In this study, approximately half of the individuals recognized on 1965 images were gone in 2003. A measure of certainty for the interpretation based on contrast values might be a fruitful approach and will be studied further in a forthcoming paper.

All the trees mapped in 2003 with a CA below $6\,m^2$ were left out of consideration in the spatial overlay since it was assumed that these individuals would be too small to be interpreted from the imagery also in 1965. However, that assumption does not necessarily hold due to the pollarding of trees (Fig. 2), the effect of which might cause the following misinterpretations in a change analysis:

- A small tree is detected in 2003 at a spot where a large tree was detected in 1965. Relying only on CA can easily create the impression that a new tree has been recruited, whereas pollarding is the true explanation for the reduced CA. Such transitions in size from a large to a small CA for individuals can easily be misinterpreted as change, particularly when changes are evaluated on the basis of a comparison of size class distributions. This can result in the false assumption that regeneration is more frequent than is actually the case.
- A large tree is detected in 2003 at a spot where no tree was detected in 1965. A large individual in 2003 appears to have been recruited after 1965, whereas, heavy pollarding had obscured its presence in the imagery (1965). This can result in the false assumption that a tree has grown rapidly or is younger than it actually is.

As seen in this study, the mere presence of trees in imagery contributes important ecological information. This study shows that 66% of the larger individuals mapped in 2003 were present in 1965, and already then they were large individuals. Correcting for trees that were probably concealed, this number might be as high as 97%. Age and growth rate in *Acacia* sp. is an unsolved problem in the literature (Hobbs, 1989; Kenneni and van der Maarel, 1990; Wyant and Reid, 1992; Springuel and Mekki, 1994; Gourlay, 1995), and the findings in this study show that these trees grow slowly and are probably very old. At the very least, it is clear that their average life-span is much longer than the 42 years estimated by Ward and Rohner (1997). Lahav-Ginott et al. (2001) used this estimate as the basis for their change analysis, thus probably biasing their interpretation, as was also pointed out by Wiegand et al. (2004), who suggest that the true age is more likely to be around 200 years. If an estimate of canopy size can be made, it can give an impression of the size distribution of a population and provide a basis for studying variation in size composition over time. It can also give a picture of the degree of pollarding if an individually based change analysis is made. Another important topic is mortality (Cole, 1989; Kenneni and van der Maarel, 1990; Ward and Rohner, 1997; Christensen, 1998; Andersen, 1999; Wiegand et al., 1999, 2000b; Krzywinski and Pierce, 2001; Shrestha et al., 2003; Bowie and Ward, 2004). Change analysis using CORONA as a historic data set can certainly contribute to this topic. Since mortality rates in the ED have apparently been high recently, the historic properties of this imagery can also make it possible to obtain a picture of an earlier, less disturbed landscape, which probably had a richer content of ecological information. This has already proved very important for archaeologists who can thereby detect sites hidden or destroyed by later developments (McDonald, 1995; Philip et al., 2002; Fowler, 2004a). Since imagery gives spatially explicit information, it also offers promising opportunities for studies of spatial patterns, making it possible to gain insight into the spatio-temporal dynamics of an arboreal population, e.g. by comparison of regeneration and mortality patterns, and local and regional patterns in relation to hydrological landscape properties.

## Acknowledgments

This work was supported by a Ph.D. Grant from the Research Council of Norway (project no. 149181/730) and the Faculty of Science, University of Bergen. Additional funding in support of fieldwork was received from Olaf Grolle Olsens Legat and L. Meltzers Høyskolefond. I thank Jonatan Krzywinski and Howaida Abd El-Rahman for assistance during fieldwork and Knut Krzywinski and Richard H. Pierce for additional help and useful discussion also during the course of the analysis and with the manuscript. Thanks also to three anonymous reviewers for useful comments.

## References

Adrados, C., Girard, I., Gendner, J.P., Janeau, G., 2002. Global positioning system (GPS) location accuracy improvement due to selective availability removal. Comptes Rendus Biologies 325, 165–170.

Alstad, G., Vetaas, O.R., 1994. The influence of *Acacia tortilis* stands on soil properties in Arid North-Eastern Sudan. Acta Oecologica 15, 449–460.

Altmaier, A., Kany, C., 2002. Digital surface model generation from CORONA satellite images. ISPRS Journal of Photogrammetry and Remote Sensing 56, 221–235.

Andersen, G.L., 1999. Change and variation in a hyper-arid cultural landscape: a methodological approach using remote sensing timeseries (LANDSAT MSS and TM, 1973–1996) from the wadi vegetation of the Eastern Desert of Egypt. Cand. Scient. Thesis, Department of Botany/NERSC, University of Bergen, p. 205.

Ball, J., 1912. The Geography and Geology of South-Eastern Egypt. Government Press, Cairo.

Batanouny, K.H., 1973. Habitat features and vegetation of deserts and semi-deserts in Egypt. Vegetatio 27, 181–199.

BenDavid-Novak, H., Schick, A.P., 1997. The response of *Acacia* tree population on small alluvial fans to changes in the hydrological regime: Southern Negev Desert, Israel. Catena 29, 341–351.

Bowie, M., Ward, D., 2004. Water and nutrient status of the mistletoe *Plicosepalus acaciae* parasitic on isolated Negev Desert populations of *Acacia raddiana* differing in level of mortality. Journal of Arid Environments 56, 487–508.

Brandtberg, T., Walter, F., 1998. Automated delineation of individual tree crowns in high spatial resolution aerial images by multiple-scale analysis. Machine Vision and Applications 11, 64–73.

Butler, B., Ali, M.R., 2000. Egypt Navigates into the DGPS era. GPS World, 30–36.

Campbell, J.B., 2002. Introduction to Remote Sensing. Taylor & Francis, London.

Chesson, P., Gebauer, R.L.E., Schwinning, S., Huntly, N., Wiegand, K., Ernest, M.S.K., Sher, A., Novoplansky, A., Weltzin, J.F., 2004. Resource pulses, species interactions, and diversity maintenance in arid and semi-arid environments. Oecologia 141, 236–253.

Christensen, A., 1998. Faham fi! Charcoal production as part of urban–rural interaction in the Red Sea Hills, Sudan. Cand. polit. Thesis, Department of Geography/Nansen Environmental and Remote Sensing Center, University of Bergen, p. 207.

Clinton, W., 1995. Executive order 12951.

Clinton, W., 2000. Statement by The President Regarding the United States' Decision to Stop Degrading Global Positioning System Accuracy. Available online from: http://www.ostp.gov/html/0053_2.html, last updated 2000.

Cloud, J., 2001. Imaging the world in a barrel: CORONA and the clandestine convergence of the earth sciences. Social Studies of Science 31, 231–251.

Cole, R., 1989. Changes in Tree Density on Five Sites, Red Sea Province: Early 1960s to 1989.

D'Eon, R.G., Serrouya, R., Smith, G., Kochanny, C.O., 2002. GPS radiotelemetry error and bias in mountainous terrain. Wildlife Society Bulletin 30, 430–439.

Eshete, G., Stahl, G., 1999. Tree rings as indicators of growth periodicity of acacias in the Rift Valley of Ethiopia. Forest Ecology and Management 116, 107–117.

Fowler, M.J.F., 2004a. Archaeology through the keyhole: the serendipity effect of aerial reconnaissance revisited. Interdisciplinary Science Reviews 29, 118–134.

Fowler, M.J.F., 2004b. Declassified CORONA KH-4B satellite photography of remains from Rome's desert frontier. International Journal of Remote Sensing 25, 3549–3554.

Goslee, S.C., Havstad, K.M., Peters, D.P.C., Rango, A., Schlesinger, W.H., 2003. High-resolution images reveal rate and pattern of shrub encroachment over six decades in New Mexico, USA. Journal of Arid Environments 54, 755–767.

Gourlay, I.D., 1995. Growth ring characteristics of some African *Acacia* species. Journal of Tropical Ecology 11, 121–140.

Hassib, M., 1950. Distribution of plant communities in Egypt. Bulletin of the Faculty of Science, Fouad I University No. 29.

Hengl, T., Jurisic, M., Martinic, I., Husnjak, S., 2001. Satellite navigation (GPS)—trends and application. Strojarstvo 43, 49–56.

Hobbs, J.J., 1989. Bedouin Life in the Egyptian Wilderness. University of Texas Press, Austin, TX.

IGEB, 2003. GPS Fluctuations Over Time on May 2, 2000. Available online from: http://www.igeb.gov/sa/diagram.shtml, last updated August 5, 2003.

Kadmon, R., Harari Kremer, R., 1999. Studying long-term vegetation dynamics using digital processing of historical aerial photographs. Remote Sensing of Environment 68, 164–176.

Kassas, M., 1952. Habitat and plant communities in the Egyptian desert I. Introduction. Journal of Ecology 40, 342–351.

Kassas, M., 1953. Habitat and plant communities in the Egyptian desert II. The features of a desert community. Journal of Ecology 41, 248–256.

Kassas, M., 1954. Habitat and plant communities in the Egyptian desert III. The wadi bed ecosystem. Journal of Ecology 42, 424–445.

Kassas, M., Zahran, M.A., 1971. Plant life on the coastal mountains of the Red Sea, Egypt. Journal of the Indian Botanical Society 50A, 571–589.

Kenneni, L., van der Maarel, E., 1990. Population ecology of *Acacia tortilis* in the semi-arid region of the Sudan. Journal of Vegetation Science 1, 419–424.

Kostka, R., 2002. The world mountain Damavand: documentation and monitoring of human activities using remote sensing data. ISPRS Journal of Photogrammetry and Remote Sensing 57, 5–12.

Krzywinski, K., Pierce, R.H. (Eds.), 2001. Deserting the Desert a Threatened Cultural Landscape between the Nile and the Sea, first ed. Bergen.

Lahav-Ginott, S., Kadmon, R., Gersani, M., 2001. Evaluating the viability of *Acacia* populations in the Negev Desert: a remote sensing approach. Biological Conservation 98, 127–137.

Laliberte, A.S., Rango, A., Havstad, K.M., Paris, J.F., Beck, R.F., McNeely, R., Gonzalez, A.L., 2004. Object-oriented image analysis for mapping shrub encroachment from 1937 to 2003 in southern New Mexico. Remote Sensing of Environment 93, 198–210.

Larsen, M., Rudemo, M., 1998. Optimizing templates for finding trees in aerial photographs. Pattern Recognition Letters 19, 1153–1162.

Leachtenauer, J., Daniel, K., Vogl, T., 1998. Digitizing satellite imagery: quality and cost considerations. Photogrammetric Engineering and Remote Sensing 64, 29–34.

Li, X., Strahler, A.H., 1985. Geometric-optical modelling of a conifer forest canopy. IEEE Transactions on Geoscience and Remote Sensing GE-23, 705–721.

Li, X., Strahler, A.H., 1986. Geometric-optical bidirectional reflectance modeling of a conifer forest canopy. IEEE Transactions on Geoscience and Remote Sensing GE-24, 906–919.

Lillesand, T.M., Kiefer, R.W., 2000. Remote Sensing and Image Interpretation. Wiley, New York.

Liu, C.J., 2002. Effects of selective availability on GPS positioning accuracy. Southern Journal of Applied Forestry 26, 140–145.

Lorenz, H., 2004. Integration of Corona and Landsat Thematic Mapper data for bedrock geological studies in the high Arctic. International Journal of Remote Sensing 25, 5143–5162.

Martin, D.M., Moss, J.M.S., 1997. Age determination of *Acacia tortilis* (Forsk.) Hayne from northern Kenya. African Journal of Ecology 35, 266–277.

McDonald, R.A., 1995. CORONA—success for space reconnaissance, a look into the cold-war, and a revolution for intelligence. Photogrammetric Engineering and Remote Sensing 61, 689–720.

Meigs, P., 1953. World distribution of arid and semi-arid homoclimates. In: Review of research in arid zone hydrology. UNESCO, Paris, pp. 203–210.

Noy-Meir, I., 1979/80. Structure and function of desert ecosystems. Israel Journal of Botany 28, 1–19.

Noy-Meir, I., 1985. Desert ecosystem structure and function. In: Evenari, M., Noy-Meir, I., Goodall, D.W. (Eds.), Hot Desert and Arid Shrublands, A. Elsevier, Amsterdam, pp. 93–104.

Philip, G., Donoghue, D., Beck, A., Galitasatos, N., 2002. CORONA satellite photography: an archaeological application from the Middle East. Antiquity 76, 109–118.

Pouliot, D.A., King, D.J., Bell, F.W., Pitt, D.G., 2002. Automated tree crown detection and delineation in high-resolution digital camera imagery of coniferous forest regeneration. Remote Sensing of Environment 82, 322–334.

Rigina, O., 2003. Detection of boreal forest decline with high-resolution panchromatic satellite imagery. International Journal of Remote Sensing 24, 1895–1912.

Rowlingson, B.S., Diggle, P.J., 1993. Splancs—spatial point pattern-analysis code in S-plus. Computers & Geosciences 19, 627–655.

Shrestha, M.K., Stock, W.D., Ward, D., Golan-Goldhirsh, A., 2003. Water status of isolated Negev desert populations of *Acacia raddiana* with different mortality levels. Plant Ecology 168, 297–307.

Sohn, H.G., Kim, G.H., Yom, J.H., 2004. Mathematical modelling of historical reconnaissance CORONA KH-4B imagery. Photogrammetric Record 19, 51–65.

Springuel, I., Mekki, A.M., 1994. Economic value of desert plants—*Acacia* trees in the wadi-allaqi biosphere reserve. Environmental Conservation 21, 41–48.

Strahler, A.H., Jupp, D.L.B., 1990. Modeling bidirectional reflectance of forests and woodlands using Boolean models and geometric optics. Remote Sensing of Environment 34, 153–166.

Täckholm, V., 1969. Öknen blommar. Generalstabens Litografiska Anstalt, Stockholm.

Tappan, G.G., Hadj, A., Wood, E.C., Lietzow, R.W., 2000. Use of Argon, Corona, and Landsat imagery to assess 30 years of land resource changes in west-central Senegal. Photogrammetric Engineering and Remote Sensing 66, 727–735.

Thomas, D.S.G., Middleton, N.J., 1994. Desertification: Exploding the Myth. Wiley, Chichester.

Ward, D., Rohner, C., 1997. Anthropogenic causes of high mortality and low recruitment in three *Acacia* tree taxa in the Negev desert, Israel. Biodiversity and Conservation 6, 877–893.

Wiegand, T., Jeltsch, F., 2000. Long-term dynamics in arid and semiarid ecosystems—synthesis of a workshop. Plant Ecology 150, 3–6.

Wiegand, T., Milton, S.J., 1996. Vegetation change in semiarid communities—simulating probabilities and time scales. Vegetatio 125, 169–183.

Wiegand, T., Milton, S.J., Wissel, C., 1995. A simulation-model for a shrub ecosystem in the semiarid karoo, South-Africa. Ecology 76, 2205–2221.

Wiegand, K., Jeltsch, F., Ward, D., 1999. Analysis of the population dynamics of *Acacia* trees in the Negev Desert, Israel with a spatially-explicit computer simulation model. Ecological Modelling 117, 203–224.

Wiegand, K., Jeltsch, F., Ward, D., 2000a. Do spatial effects play a role in the spatial distribution of desert-dwelling *Acacia raddiana*? Journal of Vegetation Science 11, 473–484.

Wiegand, K., Ward, D., Thulke, H.H., Jeltsch, F., 2000b. From snapshot information to long-term population dynamics of acacias by a simulation model. Plant Ecology 150, 97–114.

Wiegand, K., Jeltsch, F., Ward, D., 2004. Minimum recruitment frequency in plants with episodic recruitment. Oecologia 141, 363–372.

Wulder, M.A., White, J.C., Niemann, K.O., Nelson, T., 2004. Comparison of airborne and satellite high spatial resolution data for the identification of individual trees with local maxima filtering. International Journal of Remote Sensing 25, 2225–2232.

Wyant, J.G., Reid, R.S., 1992. Determining the age of *Acacia tortilis* with ring counts for South Turkana, Kenya: a preliminary assessment. African Journal of Ecology 30, 176–180.

Zahran, M.A., Willis, A.J. (Eds.), 1992. The Vegetation of Egypt. Chapman & Hall, London.